Precision of neuronal localization in 2D cell cultures by using high-performance electropolymerized microelectrode arrays correlated with optical imaging

Mahdi Ghazal, Corentin Scholaert, Corentin Dumortier, Camille Lefebvre, Nicolas Barois, Sebastien Janel, Mehmet Tarhan, Morvane Colin, Luc Buée, Sophie Halliez, et al.

PAPER • **OPEN ACCESS**

Precision of neuronal localization in 2D cell cultures by using high-performance electropolymerized microelectrode arrays correlated with optical imaging

Biomedical Physics & Engineering Express

PAPER

Precision of neuronal localization in 2D cell cultures by using high-performance electropolymerized microelectrode arrays correlated with optical imaging

Mahdi Ghazal[1], Corentin Scholaert[1], Corentin Dumortier[2], Camille Lefebvre[2], Nicolas Barois[3], Sebastien Janel[3], Mehmet Cagatay Tarhan[1], Morvane Colin[2], Luc Buée[2], Sophie Halliez[2], Sebastien Pecqueur[1], Yannick Coffinier[1], Fabien Alibart[1,4,*] and Pierre Yger[2,5,*]

[1] Institut d'Électronique, Microélectronique et Nanotechnologie (IEMN), CNRS, UMR 8520, F-59652 Villeneuve d'Ascq, France
[2] Lille Neurosciences & Cognition (lilNCog)—U1172 (INSERM, Lille), Univ Lille, CHU Lille 59045 Lille, France
[3] Univ. Lille, CNRS, Inserm, CHU Lille, Institut Pasteur Lille, U1019 - UMR 9017 - CIIL - Center for Infection and Immunity of Lille, F-59000 Lille, France
[4] Laboratoire Nanotechnologies & Nanosystèmes (LN2), CNRS, Université de Sherbrooke, J1X0A5, Sherbrooke, Canada
[5] Sorbonne Université, INSERM, CNRS, Institut de la Vision, F-75012 Paris, France
[*] Authors to whom any correspondence should be addressed.

E-mail: fabien.alibart@univ-lille.fr **and** pierre.yger@inserm.fr

OPEN ACCESS

RECEIVED
27 October 2022

REVISED
23 January 2023

ACCEPTED FOR PUBLICATION
6 February 2023

PUBLISHED
17 March 2023

Keywords: spike sorting, MEA, neuronal localization

Supplementary material for this article is available online

Abstract

Recently, the development of electronic devices to extracellularly record the simultaneous electrical activities of numerous neurons has been blooming, opening new possibilities to interface and decode neuronal activity. In this work, we tested how the use of EDOT electropolymerization to tune post-fabrication materials could optimize the cell/electrode interface of such devices. Our results showed an improved signal-to-noise ratio, better biocompatibility, and a higher number of neurons detected in comparison with gold electrodes. Then, using such enhanced recordings with 2D neuronal cultures combined with fluorescent optical imaging, we checked the extent to which the positions of the recorded neurons could be estimated solely via their extracellular signatures. Our results showed that assuming neurons behave as monopoles, positions could be estimated with a precision of approximately tens of micrometers.

1. Introduction

The growth of neurophysiology applications is leading to fundamental discoveries in communication setups for interfacing and computing the brain's electrical activity. Indeed, in recent years, the development of electronic devices such as microelectrode arrays (MEAs) for simultaneously recording the extracellularly electrical activities of single neurons up to large populations of neurons has been blooming [1]. The rationale for such an interest is that assuming one could record the activity of many neurons at the single-spike levels, the possibilities for brain-machine interfaces are tremendous [2–4]. However, to decode this neural activity and extract relevant information from the recordings obtained via these MEAs, one needs to perform a post-processing step called spike sorting (see [5] for a recent review). In a nutshell, during spike sorting, the spikes detected from the extracellular traces are differentiated according to their spatio-temporal shapes (both in amplitude and time) to isolate each individual neuron's electrical activity for a better understanding of the global dynamic of the neural network.

While spike sorting is a very active topic [6], one can notice that in most, if not all the algorithms, the differentiation of the extracellular waveforms emitted by the individual neurons is usually performed via a clustering algorithm, launched after reducing the dimensionality of the waveforms to a so-called 'feature space'. In the literature, various dimensionality reduction techniques have been used to perform this projection, such as Principal Component Analysis [7], SVD [8], and ICA [9]. All have in common to project the

waveforms into an abstract feature space, and their projections must be learned on a subset of the data before application.

Recently, however, the question of bypassing such a feature extraction step has been brought up, especially in the context of *in-vivo* nonstationary recordings, to tackle the problems of drifting tissues [6, 10]. Indeed, the possibility to quickly get a raw estimate of the position of the cells obtained from the shapes of their extracellular waveforms would potentially ease the spike sorting procedures and simplify the handling of physical drifts [11]. While, quite often, the localization of the neurons has been very naively estimated by several spike-sorting algorithms with a simple Center Of Mass (COM) algorithm depending on their electrical signatures, more evolved algorithms have been proposed to infer such positions [12–14], taking into account some physical properties of the cells. In this work, we will try to estimate how precise such localization schemes could be in 2D cell cultures when considering that cells behave as monopoles [14, 15].

Indeed, while appealing, the precision of these localization techniques has yet to be properly tested with ground truth recordings. Therefore, this is hard to know to which extent such 'estimated' positions could be used to properly estimate some true physical properties of the cells, such as drifts. In this work, we will compare how accurate such localization methods could be either with synthetic or with *in-vitro* recordings of neuronal cultures and when the spacing between electrodes is not so dense. Indeed, it is well known that increasing the density of the recordings can help the spike sorting algorithms [7, 16, 17], but at the cost of more complicated analysis pipelines. Consequently, to enhance the quality of the recordings without increasing the density, we decided to test the use of electrodes made of conducting polymers such as poly(3,4-ethylenedioxythiophene) (PEDOT). Indeed, PEDOT has recently emerged for optimizing the performance of microelectrodes due to its mixed ionic electronic conduction [18–20], biocompatibility [21], and low impedance [22–24]. Many studies showed promising results for the use of PEDOT for coating the microelectrodes of MEA as a state of art and proof of concept in enhancing the signal-to-noise ratio (SNR) [25] and the quality of the recordings [22, 26].

Here, we first report the use of EDOT electropolymerization to tune post-fabrication material and geometrical parameters of passive microelectrodes. The process optimizes the cell/electrode interface by decreasing its impedance and improving its affinity with neurons: results demonstrate an improved signal-to-noise ratio, good biocompatibility, and a higher number of neurons detected compared with gold electrodes from the same neural cultures. Secondly, by using these high-performance MEAs, we investigated the possibility of accurately estimating the positions of the neurons solely from extracellular recordings by studying the correlation between electrical activity (obtained via spike sorting) and optical imaging (Fluorescent) of neural networks cultured on MEAs. By using the SpykingCircus software [7] to spike sort the extracellular recordings, we estimated the positions of the neurons either by using the Center Of Mass of their electrical signatures or by inferring the positions assuming cells would behave as monopoles. By superposition of the fluorescent and images, we compared the observed physical positions of the neurons with the ones predicted by the two aforementioned methods. This approach showed the high accuracy of the monopole hypothesis compared to the center of mass.

2. Materials and methods

2.1. MEAs fabrication

The configuration design of the MEA contact pads and the reference electrodes is suited to the commercial MEA-System (MEA, 2100-System, Headstage for two MEAs with 60 electrodes, Multichannel Systems). Conventional optical lithography and lift-off techniques were used to pattern the gold electrodes on a glass chip. The spacing between the adjacent working electrodes is 100 μm. A 2 μm thick parylene C layer was deposited to implement a passivation layer and in order to define the openings of the 30 μm microelectrodes (58 microelectrodes), the two reference electrodes (1 mm), and the contact pads. The PEDOT:PSS conducting polymer was deposited on top of the gold microelectrodes via electropolymerization technique.

2.2. Electropolymerization materials and instrumentation

Electropolymerization was performed by potentiostatic configuration in an aqueous electrolyte containing 0.1 M of 3,4-ethylenedioxythiophene (EDOT) and 100 mM of sodium poly(sodium-4-styrene sulfonate) (NaPSS). All chemicals were purchased from Sigma Aldrich. The microelectrode (30 μm) as working electrode (V_{IN}) and reference electrode (1000 μm) as a counter electrode (V_{OUT}).

2.3. Electrochemical impedance spectroscopy (EIS)

Electrochemical impedance measurements were performed with a Solartron Analytical (Ametek) impedance analyzer from 1 MHz to 1 Hz. All measurements were done in the same electrical electrical (V_{DC} = 100 mV and V_a = 20 mV) and electrochemical conditions (PBS as electrolyte). The sensing microelectrode (30μm) as working electrode (V_{IN}) and the reference electrode (1000 μm) as V_{OUT}.

Circuit impedance modeling was performed using an open-source EIS Spectrum Analyzer software. The fitting of RC parameters was adjusted manually by simultaneous comparison of the Bode's modulus, Bode's phase and Nyquist plots.

2.4. Cell culture on MEAs

Mouse primary cortical cells were prepared from 15-days-old C57BL/6JRj mouse embryos as previously described [27]. The present experimental research has been performed with the approval of an ethical committee (agreement APAFIS#2264-2015101320441671 from CEEA75, Lille, France) and follows European guidelines for the use of animals. Gestating females (Janvier Labs) were housed in a temperature-controlled (20 °C–22 °C) room maintained on a 12 h day/night cycle with food and water provided *ad libitum*. The culture medium was made of Neurobasal (Gibco) supplemented with B-27 (Gibco), Antibiotic-Antimycotic (Gibco), and L-glutamine (Gibco). Before utilization, the MEAs were sterilized by heating in water at 125 °C for 30 min then it was kept in water. Before cell seeding, the MEAs were coated with an adhesion layer consisting of a mix of Poly-D-lysine (0.5 mg ml^{-1}, Sigma) and laminin (10 $\mu g\ ml^{-1}$, Sigma). The coating solution was applied for 30 min at room temperature and then washed using sterile water (Corning). For each MEA, one drop of a cellular suspension at 4000 cells μl^{-1} in cell culture medium was seeded on the MEA recording area (120 000 cells). Ten minutes after plating, 1 ml of fresh medium was added and the MEA culture chambers were sealed with a removable hydrophobic semipermeable membrane cover (fluorinated ethylene-propylene, 12.5 microns thick, Multi-Channel Systems). Cultures were kept in a cell incubator (ThermoScientific) at 37 °C in a 5% CO_2 atmosphere. The culture medium was never changed but small amounts of fresh medium were added once a week to compensate for medium evaporation (never more than 10% of the initial volume).

2.5. Cell viability/metabolic activity assay and cytotoxicity/cell death assay

All the materials that were investigated for the biocompatibility experiments were deposited on glass coverslips. The coverslips were then inserted into 12-well cell culture plates (Corning, USA) and then sterilized by UV exposure. The adhesion layer coating was performed with a mix of Poly-D-lysine (0.5 mg ml^{-1}, Sigma) and laminin (10 $\mu g\ ml^{-1}$, Sigma). The coating solution was applied for 2 h at room temperature then washed using sterile water (Corning) and air-dried. Mouse primary cortical cells and cell culture medium were prepared as described above. In each well, 500 000 viable cells were seeded in a 1.5 ml culture medium (131 500 cells cm^{-2}). Cultures were kept in a cell incubator (ThermoScientific) at 37 °C in a 5% CO_2 atmosphere. The culture medium was never changed, but small amounts of fresh medium were added once a week to compensate for medium evaporation (never more than 10% of the initial volume).

To assay metabolic activity/number of viable cells, cellular reduction of MTS tetrazolium into formazan was quantified using the CellTiter 96 Aq_{ueous} One Solution Cell Proliferation Assay (Promega) following the manufacturer's instructions. Cells grown on regular glass coverslips were used as a reference meaning that their metabolic activity was set as the reference value (100%). The metabolic activity of the cells grown on the other surfaces was normalized against it. To assay cell death, the release of lactate dehydrogenase (LDH) into the cell medium was quantified using the CytoTox 96 Non-radioactive Cytotoxicity Assay (Promega) following the manufacturer's instructions. Maximum LDH release was determined by adding lysis solution (9% Triton X-100) to cells grown on regular glass coverslips. Significant differences between results obtained for cells grown on glass and results obtained for other samples with the different materials were examined using the nonparametric Mann-Whitney and Wilcoxon tests, and p-values <0.05 were considered significant.

2.6. Fluorescent imaging

For the live-cell imaging, 0, 1 μM of NeuroFluor^{TM} NeuO (Stemcell technologies) was added to the cell cultures after 21 days *in vitro*. Then neurons were live-imaged using an inverted microscope (Leica DM IL LED) and a camera (MC120 HD).

2.7. Experimental setup for in-vitro extracellular recordings through MEA

A Multi Channel MEA2100-system electronic setup was used to perform *in-vitro* recordings through MEAs. The MEA2100-system has a 60 channels headstage that amplifies and digitizes the signals connected to an interface board (MCS-IFB, Multi Channel Systems). A GUI on a computer is used for real time monitoring and recording through Multi Channel Experimenter software (Multichannel Systems). To keep the temperature of the cultures at 37 °C during the recording experiment, a temperature controller (TC02, Multi Channel Systems) was used. The data were acquired at 20 kHz.

2.8. Spike sorting

The raw extracellular recordings were processed with the SpyKING CIRCUS software [7], v1.1. Default parameters were used, and by default, all the templates found by the software were kept for further analysis. To summarise briefly the algorithmic pipeline, the extracellular signal $s(t)$ on all channels is pre-processed via filtering (Butterworth filter in the range [300, 9500 Hz]), then a whitening step to get rid of spurious noise correlations. Once this is performed, snippets of activity centered on detected peaks (where the signal goes below a certain value) are collected, aligned, and clustered in order to identify the putative spatio-temporal motifs (or templates) present in the extracellular signal $s(t)$. Once these templates have been found, the signal is reconstructed as a linear sum of those via a greedy template matching procedure. The temporal width of the templates was fixed to 3 ms. By default, every channel detects the peaks higher than 6 median absolute deviations of its noise level. However,

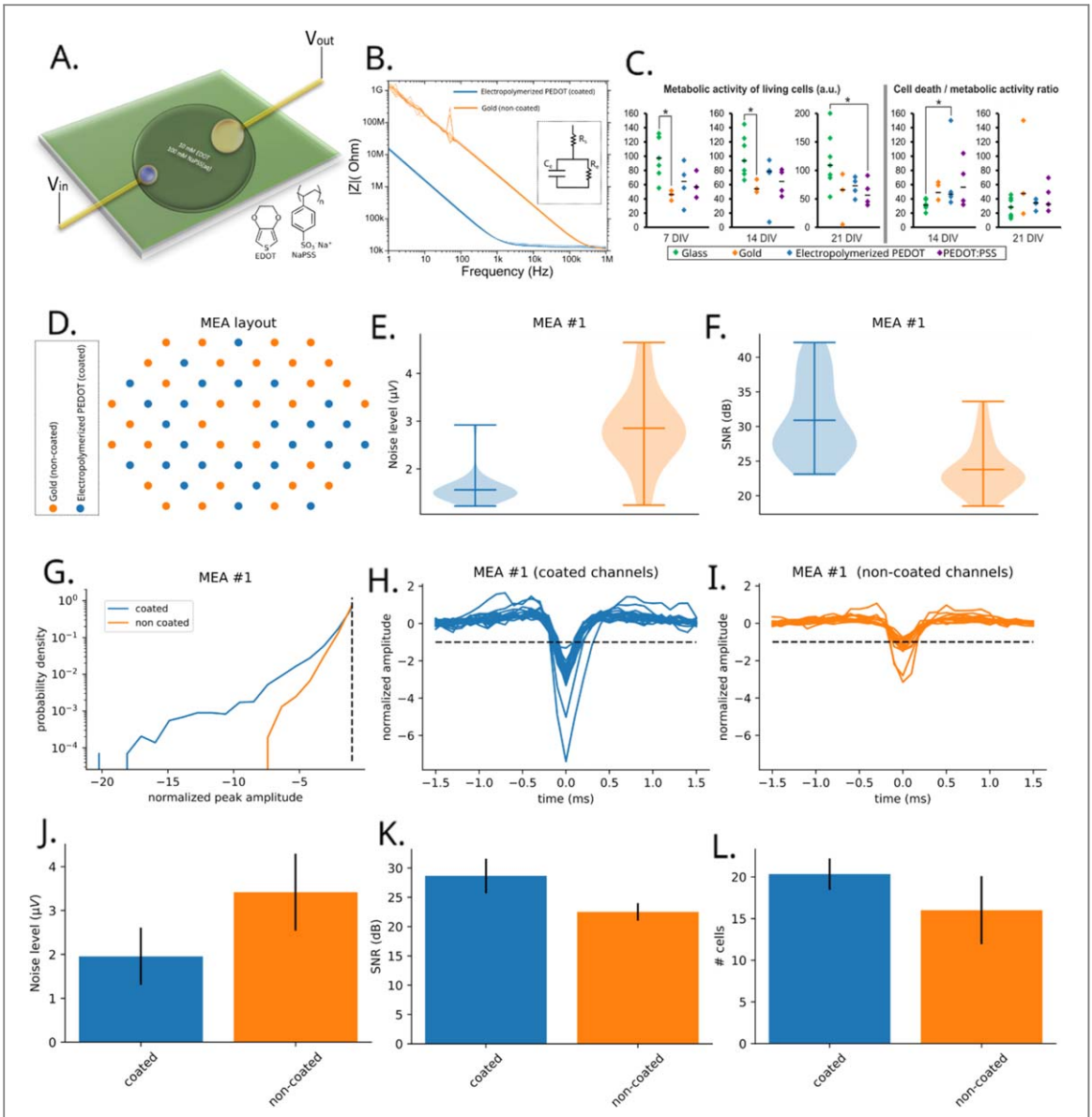

Figure 1. Effect of PEDOT coating on cell detection. (**A**) The electropolymerization setup was used to coat PEDOT on top of the gold microelectrodes. Bottom right: Chemical structures of the components introduced in the electroactive electrolytes, compromising EDOT and sodium polystyrene sulfonate (NaPSS) used as a supporting electrolyte in water. (**B**) Bode plot cure showing the impedance modulus of both non-coated (gold) and coated electrodes (electropolymerized PEDOT). Inset: Equivalent electrical circuit is used to model the impedance recorded through the microelectrode. (**C**) Biocompatibility assessment of gold, electropolymerized PEDOT, commercial spin-coated PEDOT:PSS compared to glass biocompatibility (reference) through metabolic activity assays, cell death assays, and the ratio of cell death on metabolic activity. The differences between results obtained for cells grown on glass and results obtained from other materials were examined using the non-parametric Mann-Whitney and Wilcoxon tests (*:$p < 0.05$). (**D**) The layout of the MEA, and the patterning of the coated versus non-coated channels. (**E**) Violin plot chart showing the noise levels obtained over all channels of MEA number 1, sorted by types (coated versus non coated). (**F**) Violin plot chart showing the Signal to Noise ratio (SNR) over all channels of MEA number 1, sorted by types (coated versus non coated). (**G**) Probability density of the normalized peak amplitudes over all channels of MEA number 1, sorted by types (coated versus non-coated). (**H**) Canonical waveforms obtained for spiking neurons, over coated channels, and. (**I**) non-coated channels of MEA number 1. Histograms showing the (**J**). noise levels and (**K**). SNR values obtained over all channels averaged over three different MEAs, sorted by types (coated versus non coated). Error bars show standard deviations (**L**) Histogram showing the number of cells detected after spike sorting whose template peaks are on coated or non-coated channels averaged three different MEAs (three different cell cultures). Error bars show standard deviations.

because the noise levels might vary from channel to channel, we considered in figure 1 the normalized amplitudes: every amplitude detected on a given channel is divided by the detection threshold on this particular channel. This ensured to have unitless amplitudes that could be compared across channels. In order to quickly assign templates/putative cells to electrodes (see figure 1(L)), we identified in templates the channels on which their extrema are obtained. Cells are then assumed to be close to these channels and pooled accordingly.

2.9. Synthetic templates

In order to benchmark how precise the localization of the soma can be for various methods, we generated

synthetic templates via the MEArec software [28]. Using a standard neuronexus 32 channels probe layout, with a spacing of 100 μm between channels (to copy the spacing used in the real recordings), we generated 50 templates for 50 fake neurons at random positions. The extracellular waveforms of these cells are taken from a library (see [28]) of *in vivo* excitatory/inhibitory neurons.

2.10. Estimation of the positions

To assess the putative positions of the somas, two methods are considered. The first one used a lot in the literature, is a straightforward center of mass estimation. More precisely, assuming that the neuron i has the waveform $w_i(t)$ defined on several channels $a \in \{1, .. n_{channels}\}$, we computed the peak-to-peak values $ptp_i(a)$ on every channel a. Since every channel has a physical position in the 2D space $\boldsymbol{p_a} = (\boldsymbol{x_a}, \boldsymbol{y_a})$, we can obtain, for every neuron i its barycenter or, its so-called Center of Mass (CoM_i) as

$$CoM_i = \frac{\sum_a ptp_i(a).p_a}{\sum_a ptp_i(a)}$$

The second method used in the paper is referred to as the monopole approximation. As has been done in [28] or [11], the idea is to consider the cell as a monopole and infer its position by triangulation, given the amplitudes of the templates perceived on all channels. More precisely, assuming the cell behaves as a monopole, we can exploit the fact that each spike is detectable on multiple channels a simultaneously: i.e., if the position of cell i is (x_i, y_i), we have multiple observations of the form

$$ptp_i(a) = \frac{k}{\sqrt{(x_a - x_i)^2 + (y_a - y_i)^2}}$$

Therefore, one can try to solve an optimization problem and optimize the following cost function $\Phi(x_i, y_i, k)$, finding (x_i, y_i, k) in order to minimize

$$\Phi(x_i, y_i, k) = \sum_a \left(ptp_i(a) - \frac{k}{\sqrt{(x_a - x_i)^2 + (y_a - y_i)^2}} \right)^2$$

To minimize the cost function, we used the scipy.optimize [27] toolbox with the BGFS algorithm. All cells are assumed to only have 2D coordinates, i.e. the depth is considered as fixed and equal for all neurons.

2.11. CellPose and cell localizations

In order to localise the positions of the somas on the cells, we used CellPose [28] to detect the cells from fluorescent images. More precisely, we used the trained 'livecell' model with a flow_threshold parameter of 0.6 and a cell diameter of 30 pixels.

3. Results

3.1. Effect of PEDOT coatings on cell detection

First, in order to get the most from the extracellular recordings, we wanted to check if using EDOT electropolymerization to tune post-fabrication of the electrodes could help boost the signal-to-noise ratio for the spikes recorded in the vicinity of the electrodes. For this purpose, we used microelectrode arrays fabricated with 58 gold sensing microelectrodes (30 μm diameter) and two gold reference electrodes X33 bigger in surface area (1 mm). The chip's design is similar to the commercial in-vitro MEAs, which can be used through a commercial Multichannel System (MCS). The gold metallic microelectrodes were patterned on glass chips following a conventional route through optical lithography and lift-off. A layer of Parylene C was used to define the electrode's opening and its contact pads, in addition to its use as an insulation layer. The PEDOT coatings on top of the 30 μm microelectrodes have been deposited through potentiostatic electropolymerization, as shown in figure 1(A). A 1.4 V_{DC} was applied for 8 s on the working electrode while grounding the reference electrode resulting in coating 200 nm PEDOT thickness in the center and 500 nm thickness at the edges of the opening. Figure 1(B) shows the Bode's modulus plot of the impedance spectra measured from 1 Hz to 1 MHz in an electrolyte containing Phosphate-buffered saline (PBS) solution for microelectrodes (n = 10) before and after PEDOT coating. Thanks to the increased surface area of the gold metallic electrode due to the additional coated layer and the volumetric capacitance of the coated PEDOT, notably, the value of the impedance modulus at 1 kHz changed from MΩ to kΩ range after depositing PEDOT on top of the gold microelectrodes (e.g. decreasing from 25 MΩ to 23 KΩ). To analyze the change in the electrical parameters of the microelectrode after electropolymerization, electrochemical impedance spectroscopy (EIS) modeling was made according to the equivalent circuit shown in the inset in figure 1(B). The low pass filter shown in the first part of the impedance modulus is modeled by a resistor-capacitor circuit (Ce and Re), representing the microelectrode's capacitance and resistance. The quasi-plateau represents the solution resistance Rs. This model is a typical theoretical model used to represent the electrode-electrolyte impedance [29]. The extracted values for the EIS analysis showed a clear increase in the electrode's capacitance from 110 pF to 11 nF showing improvement in the electrochemical properties of the microelectrode due to the growth of PEDOT material on its surface.

In the sensing aspect, one of the parameters that affect the coupling between the neuron and electrode is its input impedance, which represents how much voltage drop it can maintain on its node such that the lower impedance (higher capacitance), the better recordings are expected. Another important

parameter for sensing is the degree of affinity between the neuron and the electrode; henceforth, it signifies the degree of affinity between the neuron and the electrode.

Accordingly, we studied the biocompatibility study of the electropolymerized PEDOT material and compared it with several materials such as glass, gold, and commercial spin-coated PEDOT:PSS used in state-of-the-art. This experiment is performed by studying the living cell numbers (metabolic activity as a proxy for cell number) and cell death assays cultured on top of the different materials. Rat cortical cells grown on gold, electropolymerized PEDOT, and PEDOT:PSS were compared to cells grown on glass (control) after 7,14, and 21 days of culture *in vitro* (DIV). The mean metabolic activity of the cells grown on electropolymerized PEDOT was not significantly different from that of glass, contrary to gold. However, cell death increased slightly after 2 weeks of culture compared to glass. It is worth highlighting the fact that the cells grown commercial spin-coated PEDOT:PSS exhibit a significantly lower mean metabolic activity than that of electropolymerized PEDOT at DIV 7, 14, and 21. The cell death was also slightly lower at DIV 21 compared to spin-coated PEDOT:PSS. One hypothesis behind the enhanced biocompatibility of the electropolymerized PEDOT compared to spin-coated PEDOT:PSS could be correlated to a possible slight cytotoxic effect induced by the additives used during the preparation of the latter, such as (3-Glycidyloxypropyl)trimethoxysilane (GOPS) cross-linker used to improve film mechanical stability and adhesion to the substrate. For example, previous studies reported that using alternative cross-linkers other than GOPS enhances the cytotoxicity of PEDOT:PSS films [30].

Taken together, this showed a good biocompatibility of electropolymerized PEDOT coupled to a lower impedance compared to gold, demonstrating its superiority as a microelectrode material. Thanks to the versatility of the electropolymerization technique, we coated half of our MEA's electrode with electropolymerized PEDOT. As shown in figure 1(D), we coated the electrodes with random distribution to neglect the biological variability that could come from the cell growth heterogeneity. Here, we will be able to record the activity of the same neural network through microelectrodes with the two different materials allowing us to compare fairly the performances in cell detection. First, as shown in the graphs of figures 1(E) and (F), the noise level and SNR of the recordings were calculated statistically for the gold and electropolymerized microelectrodes. Remarkably, the mean average SNR value of the recorded microelectrodes through PEDOT ($\sim 27.5 \pm 4$ dB) is higher by 50% than that from gold microelectrodes ($\sim 21.5 \pm 2$ dB). For more statistical investigations, the SNR of the recordings was calculated for three different MEAs (figure 1(J)–(K)) with reproducible results showing both a global reduction of the noise (figure 1(J)) and higher SNR values (figure 1(K)) of coated electrodes compared to gold ones. Interestingly, the SNR values of the recording detected from the electropolymerized microelectrodes were higher than that for PEDOT:PSS microelectrodes and comparable with other planar microelectrodes material (Table S1) [31–36]. Nevertheless, the core of this part of the study is to show how better microelectrodes will affect cell detection through spike sorting. Hence, the microelectrodes that record data with better SNR are likely to detect more spikes with low amplitudes, which is considered to be one of the challenging tasks in spike sorting applications. To test this hypothesis, we performed spike sorting on the extracellular traces via a custom and dedicated software (Spyking-circus, see Methods), and as presented in the histogram in figure 1(L) we show how these coated microelectrodes had the ability to detect a higher number of cells (more neurons closer to the coated channels, see Methods) than gold microelectrodes from the same neural culture, recorded at the same time with the same conditions from three different MEAs (three different cell cultures). Noting that, for each MEA of these three MEAs, the number of the detecting cells by the coated channels was higher than that from the non-coated channels. Interestingly, by looking at figures 1(K) and (L), we see the relative difference in the values of SNR of the coated channels (40% higher) from non-coated is remarkably correlated to the relative difference between the number of cells detected from coated ($\sim$34% higher) and non coated channels. This points out the effect of high-performant microelectrodes on cell detecting through spike sorting applications. Here, in the upcoming parts, we will use MEAs with fully PEDOT-coated microelectrodes, and we will exploit its high-quality recordings and correlate it with optical imaging to investigate the precision of the neuronal localization of the spike sorting algorithms.

3.2. Estimation of the position from synthetic recordings

To first estimate how precise one could hope to be in estimating the putative position of a soma given its extracellular signature, we generated synthetic templates via the MEArec software [37]. The software comes with a built-in library of compartmental excitatory/inhibitory cells (mostly reconstructed from *in vivo* neurons). While simulating them with the neuron software [38], it allows (via the LFPy software [9]) to get an as accurate as possible view of the extracellular potentials at various recording sites. Figure 2(A) shows the layout of such a probe in 2D space and the position of the artificial neurons randomly generated in the vicinity of the channels. Using the MEArec software, we can visualize in figure 2(B) the extracellular signals on all channels for a given soma whose position is highlighted in figure 2(A) (blue dot).

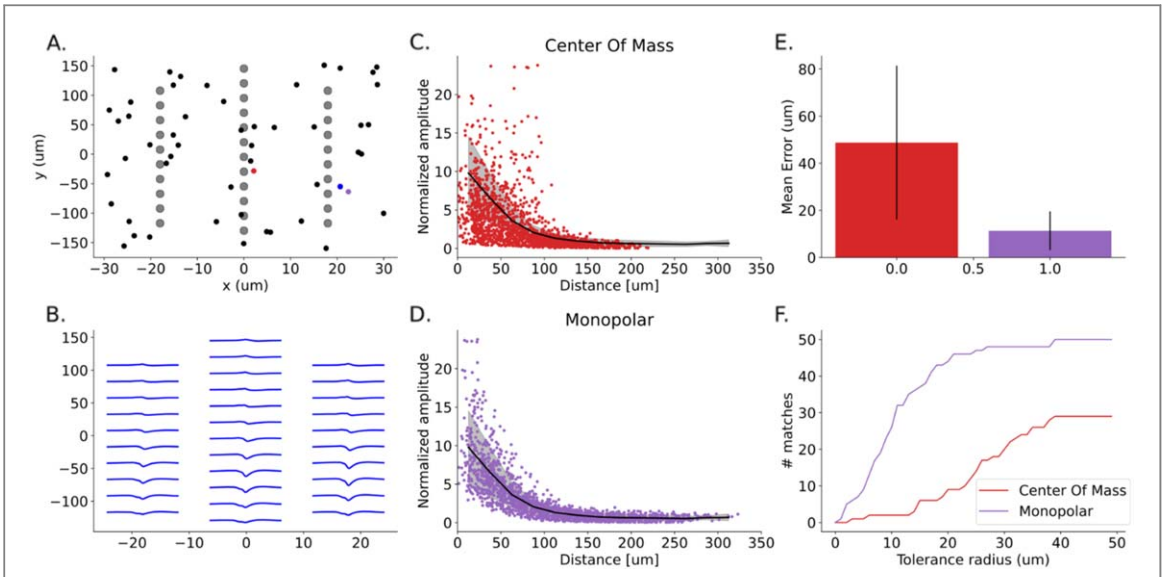

Figure 2. Estimation of the position from synthetic recordings. (**A**) The layout of a test probe (gray circles) superimposed with the position of randomly generated fake neurons (using MEArec [28]). (**B**) The waveform for one of the templates (blue dot in A). (**C**) Maximum normalized amplitudes for all the randomly generated templates, as a function of the distance between the cell positions (when estimated via the center of Mass) and the channel at which the extrema is obtained. Black lines show the theoretical curve, computed with the simulated positions. (**D**) Same but when the positions of the cells are estimated via a monopolar estimation (see Methods). (**E**) Average errors between the estimated and the physical positions of the cells, when positions are estimated either via Centre of Mass or Monopolar estimation. Error bars show the standard deviation. (**F**) The number of matches (cells such that the distance between estimated positions and ground truth physical positions are below a given tolerance radius) as a function of the tolerance radius, in μm.

As expected, the largest values of the extracellular voltages are obtained for channels next to the soma source. In figures 2(C) and (D), we show the normalized amplitudes of the templates (see Methods), on every channel, as a function of the distance between the position of the cell and the recording channels. The position of the cell is first estimated via the classical Centre of Mass procedure (COM) (see Methods, figure 2(C)), or via a more complex method assuming that the soma behaves as a monopole (see Methods, panel figure 2(D)). Because the black line in these two panels shows how the normalized amplitudes should behave given the real (artificially generated) positions, we can notice that the monopolar estimation provides a much better estimation than the theoretical estimate. Indeed, the dispersion around the black curve is smaller, and the errors are also not limited to a maximum value of 200 μm as is the case with the COM: with such an approach, it is impossible to recover positions outside the area covered by all the recording sites. The superiority of the monopolar estimation can be quantified more in-depth in figure 2(E) by comparing the average error between the real positions and their estimates (either via Center of Mass or monopolar estimation). As we can see, the error is drastically lower with the monopolar estimation. Finally, in figure 2(F), we quantified how many 'matches' could be found as a function of a given tolerance radius: a match is considered to be performed when the distance between the estimated position of a cell and the ground truth one is below a given tolerance radius. As we can see, almost all cells can be found with the monopolar estimation given a tolerance radius of 30 μm around the physical positions.

3.3. Estimation of the positions from in-vitro recordings

While this data has been obtained on artificial recordings, we can now apply the exact same analysis to some *in-vitro* recordings performed on cell cultures (see Methods). Figures 3(A) and (B) show the positions obtained after running our spike sorting software on a particular recording (DIV 21). The positions of the cells, given their Spatio-temporal extracellular signatures, are estimated either via COM (figures 2(A)) or a monopolar estimation (figure 2(B)). Strikingly, one can note that somas are much more likely to be close to recording channels in the second case. To establish if some positions are more 'plausible' than others, we displayed, in figures 3(C), (D), the amplitudes of the templates as a function of the distances between the estimated cell's position and the channels. Similar to what we observed for the synthetic recording, the distribution looks more in line with the power law and, thus, is more realistic. This can be observed at the population levels when the same distributions are plotted over numerous recordings/tissues (see figures 3(E), (F)).

3.4. Validation of the positions from in-vitro recordings

Finally, we wanted to check if the positions estimated via the monopolar estimation are good enough to rely on them accurately. The rationale behind this is that if positions can be properly inferred from the spatio-

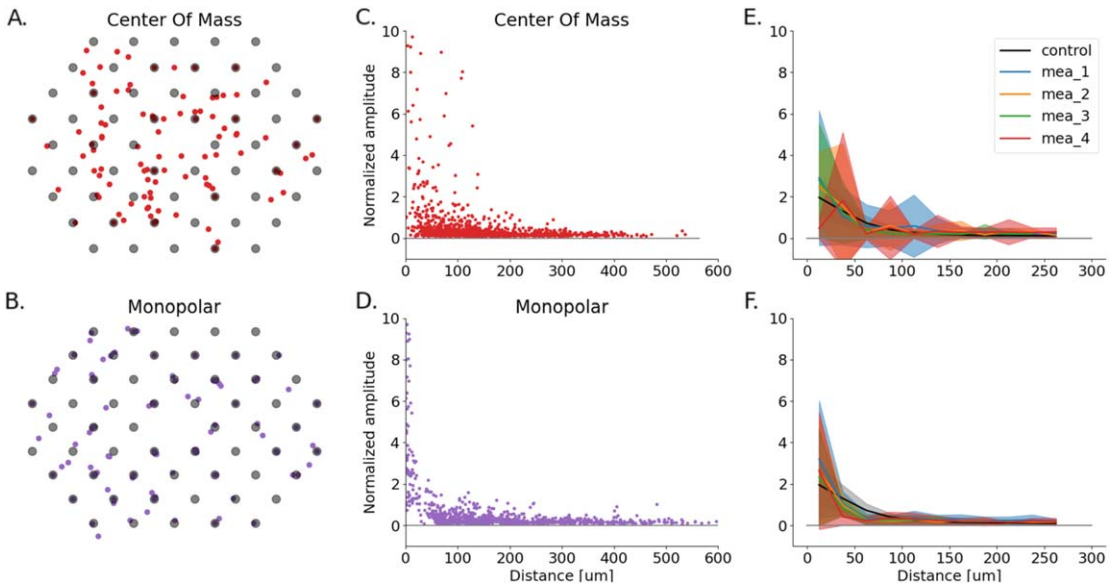

Figure 3. Estimation of the positions from *in-vitro* recordings. (**A**) The layout of the MEAs, superimposed with the positions (estimated via the Center of Mass procedure) for all the templates discovered during spike sorting via Spyking-circus [7]. (**B**) Same as A, but when positions are estimated via the monopolar estimation. (**C**) Maximum normalized amplitudes for all the randomly generated templates, as a function of the distance between the cell positions when estimated via the center of Mass and the channel at which the extrema is obtained. (**D**) Same but when the position of the cells is estimated via a monopolar estimation. (**E**) Average errors between the estimated and the physical positions of the cells, when positions are estimated either via Center of Mass. (**F**) Same as E with the Monopolar estimation.

temporal signatures in the extracellular recordings, they could be used to enhance and boost the spike sorting algorithms. We used the fluorescent imaging available for all our recordings to test that. As seen in figures 4(A), we have, for every in-vitro recording, the estimated positions of our neurons found by spike sorting superimposed on top of the MEA layout. Then, we also have the fluorescent images (see Methods) of all the living neurons co-registered to the recording sites (see figure 4(B)). Using dedicated software (see Methods), we found the putative cell bodies from the fluorescent images in order to know where the real neurons are (figure 4(C)).

Once this is achieved, we look at the probability distribution between the estimated positions of the cells and the one obtained from the fluorescent images. We iterated over all the available recordings, with positions estimated either via the COM method (figure 4(D)) or via the monopolar estimation (figure 4(E)). The black curve is a control curve obtained with randomly generated positions. While we would like, ideally, to be able to directly establish a match between the estimated position of a cell and a cell body on the fluorescent images, we realized that it was impossible for several reasons. The first one is that, as we saw in figure 2, even for synthetic recordings, the precision of the methods to estimate the position is only in the order of tens of microns. While at first glimpse, this number might seem pretty good (since this is the scale of the somas), it prevented us from establishing the matches: this is easy to find other cell bodies in the vicinity of our positions. And because the cultures are not sparse enough, and/or the recorded neurons are not particularly tagged with particular dyes, we can not have full certainty when it comes to identifying a match. Moreover, one other problem arose when looking at the data. Due to the opacity of the electrodes, the cells on top of them can not be imaged (no fluorescent signal). This is problematic because, as one can see in figure 4(A), when the positions are estimated via the monopolar estimation procedure, numerous somas are close, if not on top of the recording sites, and this can not be quantified. In figure 4(F), we naively compared the average distances between the estimated positions and the nearest cell bodies for all recordings we had. As one can see, while the monopolar method provided slightly better results, this was not drastically different. However, this is mostly because of many 'blind' neurons that can not be imaged; the method is biased towards finding matches that might be artificially far. So to compensate for this problem, we established a cutoff distance: any matches further away from that, a given radius (here 50 μm) would be discarded. By doing so, we can see in figure 4(G) that the results are much better for the monopolar estimation, with a much stronger effect.

4. Discussion

In this work, we explored the possibility of properly estimating the positions of cell bodies in neuronal

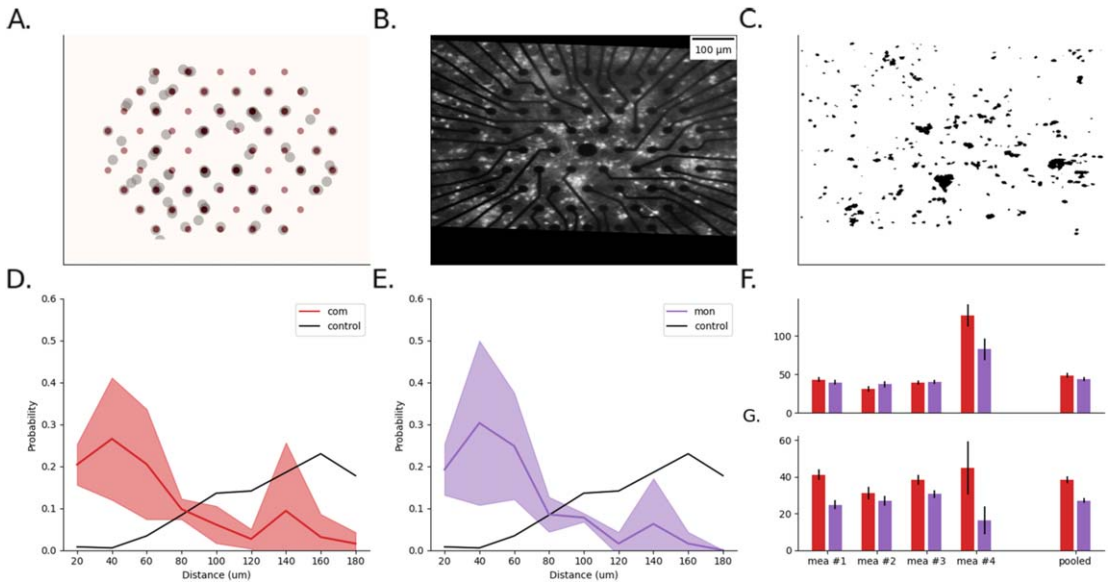

Figure 4. Validation of the positions from *in-vitro* recordings. (**A**) The layout of the MEAs (with electrodes in red), superimposed with the positions (in gray, estimated via the monopolar procedure) for all the templates discovered during spike sorting via Spyking-circus [7]. (**B**) The fluorescent image of the tissue (see Methods) co-registered to the MEA layout. (**C**) The cell bodies from B marked via CellPose (see Methods), to identify putative neurons in the recorded tissue. (**D**) Probability distribution of the distances between the positions of the neurons, estimated from extracellular signature after spike sorting and via the COM Method, and nearest somas observed in segmented images (C), averaged over 4 recordings. Red curve shows the average probability distribution, and the shaded area represents the standard deviation over experiments. The black curve is a control curve if cell positions were randomly drawn with the probe layout. (E) Same but with the monopole approximation. (F) Average distance between the positions of the neurons estimated after spike sorting (either via COM or monopole), for all individual recordings and for all pulled together. Error bars show standard deviations. (G) Same as in F, but considering only the cells whose nearby match is less than 50 μm apart (to avoid bias of non-transparent electrodes).

cultures when extracellular recordings are performed via PEDOT-coated multi-electrode arrays. Using both artificial and *in vitro* recordings, we compared two algorithmic methods to estimate the putative positions of the cell bodies simply based on the extracellular recordings of the action potentials. Being able to estimate accurately enough the positions of the somas from the extracellular signals might indeed open new possibilities in order to better understand the relationships between functional responses and morphologies of the cells. Firstly, we showed that using PEDOT coating compared to gold led to a better signal-to-noise ratio on the recording channels, and to more cells that could be spike sorted in the vicinity of these channels. Secondly, we showed that by using these low-noise recordings for spike sorting, i.e. to isolate and detect the activity of individual neurons, we could use a monopolar approximation to estimate, from the extracellular waveforms triggered on the recording devices, the putative positions of the cells.

Assuming cells were behaving as monopoles allowed us to get biologically plausible positions that seem to be more in line with the real positions of the cells, compared to simpler methods (such as center of mass, see Methods). This result was verified either with fully synthetic recordings, but also with 2D cell cultures where the physical positions of the fluorescent cells were compared to the estimated positions. Nevertheless, while our results indicate that the spatial precision of such localization methods is in the order of tens of microns (a few somas' sizes), this spatial extent should be investigated more deeply. The limits of our study were two-fold. First, it is worthwhile noting that we used a not-so-dense array, quite common in culture recordings (100 μm spacing), that gave a poor spatio-temporal resolution for the extracellular waveforms triggered by the neurons when emitting action potentials. Increasing the density of the array will clearly lead to a better resolution in estimating the cell's positions. In addition, using a denser array could also have decreased the number of cells whose positions were detected just on the top of the electrodes. This was problematic because since electrodes are not transparent, the cells can not be imaged accordingly while too close or over the recording sites, biasing the search of putative matches with the segmented fluorescent cell bodies. One solution to circumvent this particular problem could have been to use an upright microscope instead, but it was not feasible on our experimental rig. In addition, we should highlight that the monopole approximation used in this paper relies on the (strong) assumption that all the impedances of the recording channels are equal. This is likely to be false in reality, also biasing the estimated location of the somas.

The major issue with properly estimating the spatial precision of localization methods based on extracellular recordings is that the neuronal networks are always

rather dense, and thus without a proper way to tag/identify the cells recorded via spike sorting, this is hard to get an appropriate ground truth and assess with certainty which neurons are at the origin of the emitted waveforms. While the cultures in this study were also imaged via Electron Microscopy, it turned out that such an additional imaging technique did not help to identify the somas properly where the conductive microelectrodes are charged due to the electron beam leaving a blind spot above it (figure S1). To perform such unambiguous labeling, one solution could be to either go for very sparse/diluted cultures (but then the number of cultures should be improved accordingly because fewer cells are likely to be spike sorted properly) or to control exactly the position of the cells on the substrate [39] and/or guide the process outgrowth of mammalian neurons via textural guidance cues [40]. The drawback, however, is that such constrained cell morphologies might differ from what is observed *in vivo*, and thus results might only partially generalize.

Using cultures to calibrate the algorithms used to localize the cell's position reduces the influence of the depth, which can be problematic for *in-vivo* generalization. However, the validation of such localization schemes *in-vivo* has already been tested [37, 41] with ground-truth recordings from paired juxtacellular and extracellular recordings where, to a certain extent, the ground-truth location is known [42]. While the particular case of the monopole approximation was not tested, the generalization seems rather straightforward and possible, paving the way toward a proper estimation in 3D of the positions. Such estimations would be highly valuable for modern spike sorting algorithms tracking physical drifts of the cells over time in the tissues [10, 11].

5. Conclusion

In this work, we showed how using EDOT electropolymerization could optimize the cell/electrode interface to boost the signal-to-noise ratio of extracellular recordings. Using sparse and coated multielectrode arrays, we observed that the positions of the cells in 2D neuronal cultures could be estimated, from the extracellular waveforms triggered on the recording devices, with a precision of the same order of magnitude as soma's sizes. This is encouraging since increasing the density of the arrays can only refine such estimates, and it confirms the idea that inferred cell positions might be valid features that could be used to boost spike sorting algorithms, especially concerning drifts observed *in vivo*.

Acknowledgments

The authors thank the RENATECH network, and the engineers from IEMN for their support and the animal care staff of the EOPS facility (UMS-2014 US41 PLBS). This work is founded by ERC-CoG IONOS project #773 228, the LabEx DISTALZ, and the Joint Inserm-University Chairs program.

Data availability statement

The data that support the findings of this study are available upon reasonable request from the authors.

Conflict of interest

The authors declare no conflict of interest.

ORCID iDs

Mahdi Ghazal https://orcid.org/0000-0002-6027-6194

References

[1] Obien M E J *et al* 2015 Revealing neuronal function through microelectrode array recordings *Front. Neurosci.* **8 - 2014** 30
[2] Fraser G W, Chase S M, Whitford A and Schwartz A B 2009 Control of a brain–computer interface without spike sorting *J. Neural Eng.* **6** 055004
[3] Todorova S, Sadtler P, Batista A, Chase S and Ventura V 2014 To sort or not to sort: the impact of spike-sorting on neural decoding performance *J. Neural Eng.* **11** 056005
[4] Quiroga R Q, Reddy L, Koch C and Fried I 2007 Decoding visual inputs from multiple neurons in the human temporal lobe *J. Neurophysiol.* **98** 1997–2007
[5] Lefebvre B, Yger P and Marre O 2016 Recent progress in multi-electrode spike sorting methods *J. Physiol.-Paris* **110** 327–35
[6] Buccino A P, Garcia S and Yger P 2022 Spike sorting: new trends and challenges of the era of high-density probes *Prog. Biomed. Eng.* **4** 022005
[7] Yger P *et al* 2018 A spike sorting toolbox for up to thousands of electrodes validated with ground truth recordings *in vitro* and *in vivo eLife* **7** e34518
[8] Lee J *et al* 2020 YASS: Yet Another Spike Sorter applied to large-scale multi-electrode array recordings in primate retina *Neuroscience,* bioRxiv 2020.03.18.997924 preprint
[9] Lindén H, Hagen E, Łęski S, Norheim E S, Pettersen K H and Einevoll G T 2014 LFPy: a tool for biophysical simulation of extracellular potentials generated by detailed model neurons *Front. Neuroinformatics* **7** 41
[10] Steinmetz N A *et al* 2021 Neuropixels 2.0: A miniaturized high-density probe for stable, long-term brain recordings *Science* **372** eabf4588
[11] Boussard J, Varol E, Lee H D, Dethe N and Paninski L 2021 Three-dimensional spike localization and improved motion correction for Neuropixels recordings *Neuroscience* bioRxiv 2021.11.05.467503 (https://doi.org/10.1101/2021.11.05.467503)
[12] Hurwitz C L, Xu K, Srivastava A, Buccino A P and Hennig M H 2019 Scalable spike source localization in extracellular recordings using amortized variational inference arXiv:1905.12375v4 (https://doi.org/10.48550/ARXIV.1905.12375)
[13] Pettersen K H and Einevoll G T 2008 Amplitude variability and extracellular low-pass filtering of neuronal spikes *Biophys. J.* **94** 784–802
[14] Blanche T J, Spacek M A, Hetke J F and Swindale N V 2005 Polytrodes: high-density silicon electrode arrays for large-scale multiunit recording *J. Neurophysiol.* **93** 2987–3000

[15] Chelaru M I and Jog M S 2005 Spike source localization with tetrodes *J. Neurosci. Methods* **142** 305–15
[16] Pachitariu M, Steinmetz N, Kadir S, Carandini M and Kenneth D H 2016 Kilosort: realtime spike-sorting for extracellular electrophysiology with hundreds of channels, *Neuroscience,* Preprint. bioRxiv 061481 (https://doi.org/10.1101/061481)
[17] Hilgen G *et al* 2017 Unsupervised spike sorting for large-scale, high-density multielectrode arrays *Cell Rep.* **18** 2521–32
[18] Paulsen B D, Tybrandt K, Stavrinidou E and Rivnay J 2020 Organic mixed ionic–electronic conductors *Nat. Mater.* **19** 13–26
[19] Ghazal M *et al* 2022 Bio-inspired adaptive sensing through electropolymerization of organic electrochemical transistors *Adv Elect Mater.* **8** 2100891
[20] Ghazal M, Dargent T, Pecqueur S and Alibart F 2019 Addressing organic electrochemical transistors for neurosensing and neuromorphic sensing *2019 IEEE SENSORS* (Montreal, QC, Canada) 1–4
[21] Dijk G, Rutz A L and Malliaras G G 2020 Stability of PEDOT:PSS-coated gold electrodes in cell culture conditions *Adv. Mater. Technol.* **5** 1900662
[22] Middya S *et al* 2021 Microelectrode Arrays for Simultaneous Electrophysiology and Advanced Optical Microscopy *Adv. Sci.* **8** 2004434
[23] Sessolo M *et al* 2013 Easy-to-fabricate conducting polymer microelectrode arrays *Adv. Mater.* **25** 2135–9
[24] Susloparova A *et al* 2021 Low impedance and highly transparent microelectrode arrays (MEA) for *in vitro* neuron electrical activity probing *Sens. Actuators B* **327** 128895
[25] Aqrawe Z *et al* 2019 The influence of macropores on PEDOT/PSS microelectrode coatings for neuronal recording and stimulation *Sens. Actuators B Chem.* **281** 549–60
[26] Ferlauto L *et al* 2018 Development and Characterization of PEDOT:PSS/alginate soft microelectrodes for application in neuroprosthetics *Front Neurosci* **12** 648
[27] Virtanen P *et al* 2020 SciPy 1.0: fundamental algorithms for scientific computing in Python *Nat. Methods* **17** 261–72
[28] Stringer C, Wang T, Michaelos M and Pachitariu M 2021 Cellpose: a generalist algorithm for cellular segmentation *Nat. Methods* **18** 100–6
[29] Franks W, Schenker I, Schmutz P and Hierlemann A 2005 Impedance characterization and modeling of electrodes for biomedical applications *IEEE Trans. Biomed. Eng.* **52** 1295–302
[30] Solazzo M, Krukiewicz K, Zhussupbekova A, Fleischer K, Biggs M J and Monaghan M G 2019 PEDOT:PSS interfaces stabilised using a PEGylated crosslinker yield improved conductivity and biocompatibility *J. Mater. Chem. B* **7** 4811–20
[31] Wheeler B C and Nam Y 2011 *In vitro* microelectrode array technology and neural recordings *Crit. Rev. Biomed. Eng.* **39** 45–61
[32] James C D *et al* 2004 Extracellular recordings from patterned neuronal networks using planar microelectrode arrays *IEEE Trans. Biomed. Eng.* **51** 1640–8
[33] Ryynänen T *et al* 2012 Atomic layer deposited iridium oxide thin film as microelectrode coating in stem cell applications *J. Vac. Sci. Technol. Vac. Surf. Films* **30** 041501
[34] Gabay T *et al* 2007 Electro-chemical and biological properties of carbon nanotube based multi-electrode arrays *Nanotechnology* **18** 035201
[35] Kireev D, Seyock S, Lewen J, Maybeck V, Wolfrum B and Offenhäusser A 2017 Graphene multielectrode arrays as a versatile tool for extracellular measurements *Adv. Healthc. Mater.* **6** 1601433
[36] Aqrawe Z *et al* 2020 A simultaneous optical and electrical in-vitro neuronal recording system to evaluate microelectrode performance *PLoS One* **15** e0237709
[37] Buccino A P *et al* 2020 SpikeInterface, a unified framework for spike sorting *eLife* **9** e61834
[38] Hines M L and Carnevale N T 1997 The NEURON simulation environment *Neural Comput.* **9** 1179–209
[39] Micholt L, Gärtner A, Prodanov D, Braeken D, Dotti C G and Bartic C 2013 Substrate topography determines neuronal polarization and growth *in vitro PLoS One* **8** e66170
[40] Hanson J N, Motala M J, Heien M L, Gillette M, Sweedler J and Nuzzo R G 2009 Textural guidance cues for controlling process outgrowth of mammalian neurons *Lab Chip* **9** 122–13
[41] Buccino A P *et al* 2018 Combining biophysical modeling and deep learning for multielectrode array neuron localization and classification *J. Neurophysiol.* **120** 1212–32
[42] Neto J P *et al* 2016 Validating silicon polytrodes with paired juxtacellular recordings: method and dataset *J. Neurophysiol.* **116** 892–903